# Anti-windup compensator design for guidance and control of quadrotors

Majid Shahbazzadeh<sup>1</sup> and Christopher M. Richards<sup>2</sup>

Abstract-In this paper, the problem of anti-windup compensator (AWC) design for guidance and control of quadrotors in an unknown environment is addressed. Quadrotors can be affected by disturbances (such as wind), which potentially result in saturation of the propellers. When saturation occurs, the flight can become unstable, leading to a crash. On the other hand, designing an AWC to mitigate the saturation effects in the control system of a quadrotor can be a challenging task due to the heavy couplings and complex nonlinear dynamics. For this reason, we propose a new structure to design an AWC-based control system to solve this problem. Simulation results are presented in three cases: 1-without saturation, 2-with saturation - without AWC, 3-with saturation - with AWC. The effectiveness of the proposed theoretical results are verified by comparisons.

#### I. Introduction

Quadrotor unmanned aerial vehicles (UAVs) have been extensively studied and utilized due to their simple structure and vertical take-off and landing capabilities [1], [2], [3]. However, aggressive flight maneuvers and disturbances might result in actuator saturation, which significantly affects the flight quality [4]. When actuator saturation occurs, the UAV's control response may degrade, affecting its stability, and potentially leading to a crash. In recent years many studies have focused on anti-windup compensator (AWC) design for quadrotors [5], [6], [7], [8].

While the AWC is typically constructed from a linear (or linearized) model of the plant's dynamics [9], [10], [11], [12], [13], this approach is inadequate for a multiloop guidance and control architecture such as that presented in [14]. More precisely, although some recent work on attitude only control has been successfully applied to the linearized attitude dynamics about the hover operating point [15], [16], linearization of the dynamics about the hover operating point fails to provide a sufficient representation of the dynamics, especially during aggressive maneuvers and/or when wind disturbances occur. Therefore, the full nonlinear vehicle dynamics are necessary for the design of an AWCbased guidance and control system for quadrotors under these circumstances, which motivates this study.

In this paper, we present an integrated guidance and AWC-based control method for a quadrotor in a GPS-denied environment with no a priori knowledge of obstacle location. Since the coupled nonlinear dynamics of a quadrotor present challenges in the AWC design, we propose a new AWCbased control structure in which the full nonlinear dynamics can be used. The simulation results show the effectiveness and advantages of the proposed theoretical results.

The paper is arranged as follows. The problem formulation

<sup>1</sup>M. with Shahbazzadeh the Department University of chanical Engineering, Louisville, majid.shahbazzadeh@louisville.edu

<sup>2</sup>C.M. Richards is with the Department of Mechanical Engineering, University of Louisville, USA chris.richards@louisville.edu \*The material is based upon work supported by the National Science

Foundation (Award TI-2219008).

is provided in Section II. The main results are given in Section III. The simulation results are presented in Section IV. Finally, a conclusion is drawn in Section V.

## II. PROBLEM FORMULATION

First, we present the basic definitions that are needed in the sequel.

Definition 1: The saturation function  $sat(\cdot): \mathbb{R}^m \to \mathbb{R}^m$ is defined as

$$\operatorname{sat}(u)_{\underline{u}}^{\overline{u}} = \begin{cases} \overline{u} & \overline{u} < u, \\ u & \underline{u} \le u \le \overline{u}, \\ \underline{u} & u < \underline{u}, \end{cases}$$
 (1)

where  $\overline{u}$  and  $\underline{u}$  are, respectively, the upper and lower saturation limits of u.

Definition 2: The deadzone function  $Dz(\cdot)$  is defined as

$$Dz_{u}^{\overline{u}}(u) := u - \operatorname{sat}_{u}^{\overline{u}}(u). \tag{2}$$

 $\mathrm{Dz}_{\underline{u}}^{\overline{u}}(u):=u-\mathrm{sat}_{\underline{u}}^{\overline{u}}(u). \tag{2}$  The translational dynamics of a quadrotor with constrained thrust in the inertial frame are expressed as

$$\ddot{x} = -\operatorname{sat}_{\underline{T}}^{\overline{T}}(T) \left( \operatorname{c}_{\phi} \operatorname{s}_{\theta} \operatorname{c}_{\psi} + \operatorname{s}_{\phi} \operatorname{s}_{\psi} \right) / m,$$

$$\ddot{y} = -\operatorname{sat}_{\underline{T}}^{\overline{T}}(T) \left( \operatorname{c}_{\phi} \operatorname{s}_{\theta} \operatorname{s}_{\psi} - \operatorname{s}_{\phi} \operatorname{c}_{\psi} \right) / m,$$

$$\ddot{z} = g - \operatorname{sat}_{T}^{\overline{T}}(T) \operatorname{c}_{\phi} \operatorname{c}_{\theta} / m.$$
(3)

where m is the mass of the vehicle, T is the total propeller thrust perpendicular to the plane of the vehicle,  $s_{\delta} = \sin \delta$ , and  $c_{\delta} = \cos \delta$ . Note that since  $T \geq 0 \ \forall t$ , therefore  $\underline{T} = 0$ . The rotational dynamics of a quadrotor with constrained body torques in the body frame are described by

$$I\dot{\omega} + \omega \times I\omega = \operatorname{sat}_{\tau}^{\overline{\tau}}(\tau),$$
 (4)

where  $\omega = [\omega_1, \omega_2, \omega_3]^{\mathrm{T}}$  is the angular velocity vector,  $I = \mathrm{diag}\{I_1, I_2, I_3\}$  is the diagonal inertia matrix, and  $\tau = [\tau_1, \tau_2, \tau_3]^{\mathrm{T}}$  is the control torque vector.

Equation (4) can be written as

$$I_i \dot{\omega}_i = \Omega_i + \operatorname{sat}_{\tau_i}^{\overline{\tau}_i}(\tau_i), \quad i = 1, 2, 3,$$
 (5)

where

$$\begin{bmatrix} \Omega_1 \\ \Omega_2 \\ \Omega_3 \end{bmatrix} = \begin{bmatrix} (I_2 - I_3) \, \omega_2 \omega_3 \\ (I_3 - I_1) \, \omega_1 \omega_3 \\ (I_1 - I_2) \, \omega_1 \omega_2 \end{bmatrix}.$$

The vector  $\omega$  can be expressed as

$$\omega = Q\dot{\Phi},\tag{6}$$

where

$$Q = \begin{bmatrix} 1 & 0 & -\mathbf{s}_{\theta} \\ 0 & \mathbf{c}_{\phi} & \mathbf{s}_{\phi}\mathbf{c}_{\theta} \\ 0 & -\mathbf{s}_{\phi} & \mathbf{c}_{\phi}\mathbf{c}_{\theta} \end{bmatrix}, \quad \Phi = \begin{bmatrix} \phi \\ \theta \\ \psi \end{bmatrix}, \quad (7)$$

and  $\Phi$  is the vector of Euler angles. For all  $\theta \neq \pm \pi/2$ , the vector  $\Phi$  can be obtained as

$$\dot{\Phi} = Q^{-1}\omega. \tag{8}$$

Assumption 1: It is assumed that  $\phi(t) \in (-\pi/2, \pi/2)$  and  $\theta(t) \in (-\pi/2, \pi/2) \ \forall t.$ 

## III. MAIN RESULTS

This section is devoted to a guidance and control approach for a quadrotor to avoid obstacles and reach a desired destination while accounting for input saturation. The guidance and nominal control are based upon the multi-loop guidance and control architecture presented in [14]. In the following, we first design an AWC-based control for the quadrotor, and then the guidance method is presented.

# A. AWC-based control

In this subsection, we design an AWC-based controller for the rotational and translational dynamics, respectively.

The structure of the AWC-based attitude controller (see Fig. 1(a)) is considered as follows:

$$\tau_i = \tau_{\beta_i} + \tau_{Ci} + \tau_{Ai},\tag{9}$$

 $\tau_{\beta_i} = -\Omega_i + I_i \dot{\omega}_{di}, \tau_{Ci} = -K_{\omega i} e_{\omega i}, \tau_{Ai} = -K_{ai} \operatorname{Dz}_{\mathcal{I}_i}^{\overline{\tau}_i}(\tau_i),$ and  $K_{\omega i}, K_{ai}$  are positive scalars,  $e_{\omega i} := \omega_i - \omega_{di}$  where  $\omega_{di}$  is the desired angular velocity.

As can be seen, the controller consists of three terms. The first term,  $\tau_{\beta}$ , is for canceling nonlinear terms and generating error dynamics. The second term,  $\tau_C$ , is to guarantee the asymptotically stability of the error dynamics when there is no saturation, and the third term,  $\tau_A$ , is a static AWC to account for saturation.

The proof of asymptotic stability of the closed-loop system is challenging due to the input saturation constraint. In order to solve this problem, we introduce a new structure to design the AWC-based controller (see. Fig. 1(b)). Note that since  $\mathrm{Dz}_{\mathcal{I}_i}^{\overline{\tau}_i}(\tau_{\beta_i}+\tau_{C_i}+\tau_{A_i})=\mathrm{Dz}_{\mathcal{I}_i}^{\overline{\tau}_i-\tau_{\beta_i}}(\tau_{C_i}+\tau_{A_i})$ , the application of this identify to (9) does not change the controller.

For the sake of brevity, we define  $\underline{\tau}_{ni} := \underline{\tau}_i - \tau_{\beta_i}$  and  $\overline{\tau}_{ni} := \overline{\tau}_i - \tau_{\beta_i}$ . Then, according to Fig. 1(b), (5) can be rewritten as follows:

$$I_i \dot{\omega}_i = \Omega_i + \tau_{\beta_i} + \operatorname{sat}_{\underline{\tau}_{ni}}^{\overline{\tau}_{ni}} (\tau_{C_i} + \tau_{A_i}). \tag{10}$$

Substituting (2) into (10) yields

$$I_i \dot{\omega}_i = \Omega_i + \tau_i - Dz_{\tau_{n,i}}^{\overline{\tau}_{n,i}} (\tau_{Ci} + \tau_{Ai}). \tag{11}$$

Inserting (9) into (11) leads to the rotational error dynamics:

$$I_i \dot{e}_{\omega_i} = -K_{\omega_i} e_{\omega_i} - (K_{ai} + 1) \operatorname{Dz}_{\underline{\tau}_{ni}}^{\overline{\tau}_{ni}} (\tau_{C_i} + \tau_{A_i}). \quad (12)$$

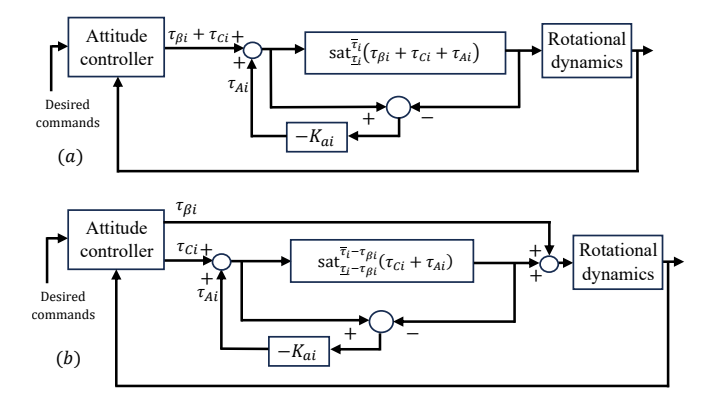


Fig. 1. (a) The AWC-based control structure with  $sat(\cdot)$ , (b) The proposed AWC-based control structure with the revised  $sat(\cdot)$ .

Now, let us consider the following Lyapunov function candidate:

$$V(e_{\omega_i}) = \frac{1}{2} I_i e_{\omega_i}^2, \quad i = 1, 2, 3$$
 (13)

Calculating the time-derivative of  $V(e_{\omega})$  along the solutions of (12) leads to

$$\dot{V}(e_{\omega i}) = e_{\omega i} I_i \dot{e}_{\omega_i} = 
e_{\omega i} [-K_{\omega i} e_{\omega i} - (K_{ai} + 1) \operatorname{Dz}_{\tau_{\alpha i}}^{\overline{\tau}_{ni}} (\tau_{Ci} + \tau_{Ai})].$$
(14)

If  $\mathrm{Dz}_{\underline{\tau}_{ni}}^{\overline{\tau}_{ni}}(\tau_{Ci}+\tau_{Ai})=0$ , (14) can be simplified to

$$\dot{V}(e_{\omega i}) = -K_{\omega i} e_{\omega i}^2. \tag{15}$$

In this case, the asymptotic stability of the rotational error dynamics is ensured for  $K_{\omega_i} > 0$ . In addition, if  $Dz_{\tau_{ni}}^{\tau_{ni}}(\tau_{C_i} +$  $\tau_{Ai} \neq 0$ , the following sector condition is satisfied for  $\overline{\tau}_{ni} > 0$ 0 and  $\underline{\tau}_{ni} < 0$ :

$$\operatorname{sat}_{\underline{\tau}_{ni}}^{\overline{\tau}_{ni}}(\tau_{Ci} + \tau_{Ai}) \mathcal{W}_{i} \operatorname{Dz}_{\underline{\tau}_{ni}}^{\overline{\tau}_{ni}}(\tau_{Ci} + \tau_{Ai}) > 0, \tag{16}$$

where  $W_i > 0$ .

Condition (16) can be rewritten as

$$\left[\tau_{C_i} + \tau_{A_i} - \mathrm{Dz}_{\underline{\tau}_{ni}}^{\overline{\tau}_{ni}} (\tau_{C_i} + \tau_{A_i})\right] \mathcal{W}_i \mathrm{Dz}_{\underline{\tau}_{ni}}^{\overline{\tau}_{ni}} (\tau_{C_i} + \tau_{A_i}) > 0.$$

$$(17)$$

According to (9), condition (17) can be rewritten as

$$[-K_{\omega i}e_{\omega i} - (K_{ai} + 1)\operatorname{Dz}_{\underline{\tau}_{ni}}^{\overline{\tau}_{ni}}(\tau_{Ci} + \tau_{Ai})] *$$

$$\mathscr{W}_{i}\operatorname{Dz}_{\underline{\tau}_{-i}}^{\overline{\tau}_{ni}}(\tau_{Ci} + \tau_{Ai}) > 0.$$
(18)

By combining (14) and (18), we can deduce that  $\dot{V}(e_{\omega i}) < 0$ 

$$\eta_{i}^{\mathrm{T}} \underbrace{\begin{bmatrix} -K_{\omega i} & -\frac{1}{2}(K_{ai} + 1 + K_{\omega i} \mathscr{W}_{i}) \\ * & -(K_{ai} + 1) \mathscr{W}_{i} \end{bmatrix}}_{\Upsilon_{i}} \eta_{i} \leq 0, \quad (19)$$

where  $\eta_i = [e_{\omega_i} \quad \mathrm{Dz}_{\underline{\tau}_{ni}}^{\overline{\tau}_{ni}} (\tau_{C_i} + \tau_{A_i})]^\mathrm{T}$ . Pre- and post-multiplying both sides of  $\Upsilon_i < 0$  by  $\mathrm{diag}\{1, \mathscr{W}_i^{-1}\}$  yields

$$\begin{bmatrix} -K_{\omega_i} & -\frac{1}{2}(K_{a_i}\mathcal{W}_i^{-1} + \mathcal{W}_i^{-1} + K_{\omega_i}) \\ * & -(K_{a_i}\mathcal{W}_i^{-1} + \mathcal{W}_i^{-1}) \end{bmatrix} \le 0.$$
 (20)  
By letting  $V_i = \mathcal{W}_i^{-1}$  and  $Y_i = K_{a_i}\mathcal{W}_i^{-1}$ , we have

$$\begin{bmatrix} -K_{\omega i} & -\frac{1}{2}(Y_i + V_i + K_{\omega i}) \\ * & -(Y_i + V_i) \end{bmatrix} \le 0.$$
 (21)

Finally, the AWC gains are obtained as  $K_{a_i} = Y_i V_i^{-1}$ . It should be noted that  $V_i$  and  $Y_i$  are positive because  $\mathcal{W}_i$  and  $K_{ai}$  are positive. Also, by choice of the Lyapunov function (13), LMI (21) for i = 1, 2, 3 is independent of the system parameters, so the result of solving it is the same for i =1, 2, 3.

Remark 1: The sector condition (16) is not satisfied for the following two cases because  $\operatorname{sat}_{\tau_{ni}}^{\overline{\tau}_{ni}}(\tau_{Ci} + \tau_{Ai})$  and  $\mathrm{Dz}_{\underline{\tau}_{ni}}^{\overline{\tau}_{ni}}(\tau_{Ci}+\tau_{Ai})$  do not have the same sign:

- $\tau_{Ci}^{-n} + \tau_{Ai} > \overline{\tau}_{ni}$  where  $\overline{\tau}_{ni} < 0$ ,
- $\tau_{Ci} + \tau_{Ai} < \underline{\tau}_{ni}$  where  $\underline{\tau}_{ni} > 0$ .

If the above conditions occur, the following inequality is used

$$[\lambda_i e_{\omega_i} - Dz_{\underline{\tau}_{ni}}^{\overline{\tau}_{ni}} (\tau_{C_i} + \tau_{A_i})] \mathscr{W}_i Dz_{\underline{\tau}_{ni}}^{\overline{\tau}_{ni}} (\tau_{C_i} + \tau_{A_i}) > 0.$$
(22)

By adding the left-hand side of (22) to (14), we can conclude

that  $\dot{V}(e_{\omega_i}) < 0$  if

$$\eta_i^{\mathrm{T}} \begin{bmatrix} -K_{\omega i} & -\frac{1}{2}(K_{ai} + 1 - \lambda_i \mathscr{W}_i) \\ * & -\mathscr{W}_i \end{bmatrix} \eta_i \le 0, \qquad (23)$$

$$\lambda_i \mathscr{W}_i e_{\omega i} \operatorname{Dz}_{\underline{\tau}_{ni}}^{\overline{\tau}_{ni}} (\tau_{Ci} + \tau_{Ai}) - \mathscr{W}_i \operatorname{Dz}_{\underline{\tau}_{ni}}^{\overline{\tau}_{ni}^2} (\tau_{Ci} + \tau_{Ai}) > 0.$$
(24)

Letting  $\overline{\lambda}_i = \lambda_i \mathcal{W}_i$  in (23) and (24) leads to

$$\eta_i^{\mathrm{T}} \begin{bmatrix} -K_{\omega_i} & -\frac{1}{2}(K_{a_i} + 1 - \overline{\lambda}_i) \\ * & -\mathcal{W}_i \end{bmatrix} \eta_i \le 0, \qquad (25)$$

and

$$\bar{\lambda}_i e_{\omega i} \mathrm{Dz}_{\underline{\tau}_{ni}}^{\overline{\tau}_{ni}} (\tau_{Ci} + \tau_{Ai}) - \mathcal{W}_i \mathrm{Dz}_{\underline{\tau}_{ni}}^{\overline{\tau}_{ni}^2} (\tau_{Ci} + \tau_{Ai}) \ge 0. \tag{26}$$

Therefore, when the sector condition (16) is not satisfied, the LMIs (25) and (26) need to be solved online. In this case,  $K_{\omega i}$  and  $K_{ai}$  are the controller and the AWC gains, respectively.

Now, we want to examine the closed-loop translational dynamics in the z-direction. Similar to above, the proposed structure in Fig. 1(b) is used to design an AWC-based thrust controller as follows:

$$T = T_{\beta} + T_C + T_A,\tag{27}$$

where

$$\begin{split} T_{\beta} &= \frac{m(g - \dot{\mathbf{w}}_d)}{\mathrm{c}\phi\mathrm{c}\theta}, \ T_C = \frac{m}{\mathrm{c}\phi\mathrm{c}\theta}K_{\mathrm{w}}e_{\mathrm{w}}, \\ T_A &= -K_{\bar{a}}\operatorname{Dz}_{T - T_{\beta}}^{\overline{T} - T_{\beta}}(T_C + T_A). \end{split}$$

 $K_{\omega}, K_{\bar{a}}$  are positive scalars,  $e_{\omega} := \omega - \omega_d$ , and  $\omega$  and  $\omega_d$ are the velocity and desired velocity of in the z direction, respectively. The desired velocity  $w_d$  is provided by the guidance discussed later in Section III-C.

For brevity, we define  $\underline{T}_n := \underline{T} - T_\beta$  and  $\overline{T}_n := \overline{T} - T_\beta$ . Then the third equation in (3) can be rewritten as:

$$\ddot{z} = g - \frac{T_{\beta}}{m} c_{\phi} c_{\theta} - \frac{\operatorname{sat}_{\underline{T}_{n}}^{\overline{T}_{n}} (T_{C} + T_{A})}{m} c_{\phi} c_{\theta}.$$
 (28)

$$\ddot{z} = g - \frac{T}{m} c_{\phi} c_{\theta} + \frac{Dz_{\underline{T}_n}^{\overline{T}_n} (T_C + T_A)}{m} c_{\phi} c_{\theta}.$$
 (29)

Inserting (27) into (29) leads

$$\dot{e}_{\omega} = -K_{\omega}e_{\omega} + (\frac{1+K_{\bar{a}}}{m})c_{\phi}c_{\theta}Dz_{\underline{T}_{n}}^{\overline{T}_{n}}(T_{C} + T_{A}).$$
 (30)

We consider the Lyapunov function candidate as:

$$V(e_{\omega}) = \frac{1}{2}e_{\omega}^{2}.$$
 (31)

Taking the derivative of  $V(e_{\omega})$  along the solutions of (30) vields

$$\dot{V}(e_{w}) = e_{w}\dot{e}_{w} = 
e_{w}(-K_{w}e_{w} + (\frac{1+K_{\bar{a}}}{m})c_{\phi}c_{\theta}Dz_{\underline{T}_{n}}^{\overline{T}_{n}}(T_{C} + T_{A})).$$
(32)

If  $Dz_T^{\overline{T}_n}(T_C + T_A) = 0$ , (32) can be simplified as

$$\dot{V}(e_{\mathbf{w}}) = -K_{\mathbf{w}}e_{\mathbf{w}}^{2}.\tag{33}$$

In this case, the asymptotic stability of the translational error dynamics in the z direction is guaranteed for  $K_{\omega} > 0$ .

On the other hand, if  $\operatorname{Dz}_{T_n}^{\overline{T}_n}(T_C + T_A) \neq 0$ , the following

sector condition is fulfilled for  $\overline{T}_{ni} > 0$  and  $\underline{T}_{ni} < 0$ :

$$\operatorname{sat}_{\underline{T}_n}^{\overline{T}_n}(T_C + T_A) \widehat{\mathscr{W}} \operatorname{Dz}_{\underline{T}_n}^{\overline{T}_n}(T_C + T_A) > 0, \qquad (34)$$

where  $\hat{W} >$ 

The above condition is equivalent to

$$[T_C + T_A - \operatorname{Dz}_{\underline{T}_n}^{\overline{T}_n} (T_C + T_A)] \widehat{\mathscr{W}} \operatorname{Dz}_{\underline{T}_n}^{\overline{T}_n} (T_C + T_A) > 0.$$
(35)

According to (27), condition (35) can be rewritten as

$$\left[\frac{m}{c\phi c\theta}K_{w}e_{w}-(1+K_{\bar{a}})\operatorname{Dz}_{\underline{T}_{n}}^{\overline{T}_{n}}(T_{C}+T_{A})\right]*$$

$$\hat{\mathscr{W}}\operatorname{Dz}_{T_{-}}^{\overline{T}_{n}}(T_{C}+T_{A})>0.$$
(36)

Based on Assumption 1, we have  $(c\phi c\theta)^2 > 0 \ \forall t$ . Multiplying (36) by  $(c\phi c\theta)^2$  results in

$$[mK_{\omega}e_{\omega} - (1 + K_{\bar{a}})c\phi c\theta \operatorname{Dz}_{\underline{T}_{n}}^{\overline{T}_{n}}(T_{C} + T_{A})] *$$

$$\hat{\mathscr{W}}c\phi c\theta \operatorname{Dz}_{T_{n}}^{\overline{T}_{n}}(T_{C} + T_{A}) > 0.$$
(37)

After adding the left-hand side of (37) to (32), we can conclude that  $\dot{V}(e_{\omega}) < 0$  if

$$\xi^{\mathrm{T}} \underbrace{\begin{bmatrix} -K_{\omega} & \frac{1}{2} [(1+K_{\bar{a}})/m + mK_{\omega} \hat{\mathscr{W}}] \\ * & -(1+K_{\bar{a}}) \hat{\mathscr{W}} \end{bmatrix}}_{\Pi} \xi \leq 0, \quad (38)$$

where  $\xi = [e_w \ \mathrm{Dz}_T^{T_n}(T_C + T_A)\mathrm{c}\phi\mathrm{c}\theta]^\mathrm{T}$ . Pre- and postmultiplying both sides of  $\Pi < 0$  by diag $\{1, \hat{W}^{-1}\}$  results

$$\begin{bmatrix} -K_{\omega} & \frac{1}{2} [(1 + K_{\bar{a}}) \hat{\mathcal{W}}^{-1} / m + m K_{\omega}] \\ * & -(1 + K_{\bar{a}}) \hat{\mathcal{W}}^{-1} \end{bmatrix} \le 0, \tag{39}$$

Finally, letting  $\hat{V} = \hat{\mathcal{W}}^{-1}$  and  $\hat{Y} = K_{\bar{a}} \hat{\mathcal{W}}^{-1}$  results in

$$\begin{bmatrix} -K_{\omega} & \frac{1}{2} [(\hat{V} + \hat{Y})/m + mK_{\omega}] \\ * & -(\hat{V} + \hat{Y}) \end{bmatrix} \le 0.$$
 (40)

After solving the above LMI, the AWC gain is calculated as  $K_{\bar{a}} = \hat{Y}\hat{V}^{-1}$ . It should be mentioned that  $\hat{V}$  and  $\hat{Y}$  are positive because  $\hat{W}$  and  $K_{\bar{a}}$  are positive.

Remark 2: Similar to Remark 1, the sector condition (34) does not hold for the following two cases:

•  $T_C + T_A > \overline{T}_n$  where  $\overline{T}_n < 0$ , •  $T_C + T_A < \underline{T}_n$  where  $\underline{T}_n > 0$ . In these cases, the following condition is employed:

$$\left[\sigma e_{w} - c\phi c\theta \operatorname{Dz}_{\underline{T}_{n}}^{\overline{T}_{n}}(T_{C} + T_{A})\right] \hat{\mathscr{W}} c\phi c\theta \operatorname{Dz}_{\underline{T}_{n}}^{\overline{T}_{n}}(T_{C} + T_{A}) > 0.$$
(41)

By combining the left hand-side of (41) and (32), we can deduce that  $V(e_{\omega}) < 0$  if

$$\xi^{\mathrm{T}} \begin{bmatrix} -K_{\omega} & \frac{1}{2} [(1+K_{\bar{a}})/m + \sigma \hat{\mathcal{W}}] \\ * & -\hat{\mathcal{W}} \end{bmatrix} \xi \leq 0.$$
 (42)

Letting  $\overline{\sigma} = \sigma \hat{\mathscr{W}}$  into (42) and (41), respectively, results in

$$\xi^{\mathrm{T}} \begin{bmatrix} -K_{\omega} & \frac{1}{2} [(1+K_{\bar{a}})/m + \bar{\sigma}] \\ * & -\hat{\mathcal{W}} \end{bmatrix} \xi \le 0, \qquad (43)$$

$$\bar{\sigma}e_{w}c\phi c\theta Dz_{\underline{T}_{n}}^{\overline{T}_{n}}(T_{C}+T_{A}) - \hat{\mathscr{W}}[c\phi c\theta Dz_{\underline{T}_{n}}^{\overline{T}_{n}}(T_{C}+T_{A})]^{2} > 0$$
(44)

In this case,  $K_{\omega}$  and  $K_{\bar{a}}$  are the controller and the AWC gains, respectively.

Remark 3: Except the cases mentioned in Remarks 1 and 2, all other cases lead to satisfaction of the conditions (16) and (34).

#### B. Guidance

In this paper, the guidance method includes two components borrowed from [14]:

- Obstacle avoidance (repulsive) component,
- Destination seeking (attractive) component.

These two components make up velocity commands  $u_c$ ,  $v_c$ , and  $w_c$  in the x-, y-, and z-directions, respectively

$$\begin{bmatrix} u_c \\ v_c \\ w_c \end{bmatrix} = \begin{bmatrix} u_{\text{rep}} \\ v_{\text{rep}} \\ w_{\text{rep}} \end{bmatrix} + \begin{bmatrix} u_{\text{attr}} \\ v_{\text{attr}} \\ w_{\text{attr}} \end{bmatrix}. \tag{45}$$

We now present the repulsive and attractive components

• Obstacle avoidance (repulsive component). To generate the obstacle avoidance component of the velocity commands, the following ellipsoids are defined in  $\mathbb{R}^3$  as:

$$E_{i} := \left\{ (x_{i}, y_{i}, z_{i}) \in \mathbb{R}^{3} : \frac{x_{i}^{2}}{a_{i}^{2}} + \frac{y_{i}^{2}}{b_{i}^{2}} + \frac{z_{i}^{2}}{c_{i}^{2}} \leq 1 \right\},$$

$$E_{o} := \left\{ (x_{o}, y_{o}, z_{o}) \in \mathbb{R}^{3} : \frac{x_{o}^{2}}{a_{o}^{2}} + \frac{y_{o}^{2}}{b_{o}^{2}} + \frac{z_{o}^{2}}{c_{o}^{2}} \leq 1 \right\}.$$

$$(46)$$

where  $E_i$  and  $E_o$  are inner and outer ellipsoids of a potential field, respectively. By using (46), the potential field is considered as

$$U(p_i) = \begin{cases} 0, & \text{if } p_i \in \mathbb{R}^3 \backslash E_o, \\ U_{\text{max}} \left( \frac{r_o(p_i) - ||p_i||}{r_o(p_i) - r_i(p_i)} \right), & \text{if } p_i \in E_o \backslash E_i, \\ U_{\text{max}}, & \text{if } p_i \in E_i, \end{cases}$$
(47)

where  $U_{\rm max}>0$  is the maximum potential, and  $p_i$  is the position of ith obstacle relative to the vehicle's center of mass, which is resolved in the body frame. In addition,  $r_{\rm i}(p_i)$  and  $r_{\rm o}(p_i)$  are defined in [14].

Next, the repulsive component is defined as

$$\begin{vmatrix} u_{\text{rep}} \\ v_{\text{rep}} \\ w_{\text{rep}} \end{vmatrix} = -\frac{1}{n_{\text{e}}} \sum_{i=1}^{n} U(p_i) \frac{\mathcal{O}^{\text{T}} p_i}{\|p_i\|}, \tag{48}$$

where  $n_e$  is the number of obstacle points contained in  $E_o$ , and  $\Theta$  is the orientation matrix of the body frame relative to the inertial frame.

$$\Theta = \begin{bmatrix}
c_{\theta}c_{\psi} & c_{\theta}s_{\psi} & -s_{\theta} \\
s_{\phi}s_{\theta}c_{\psi} - c_{\phi}s_{\psi} & s_{\phi}s_{\theta}s_{\psi} + c_{\phi}c_{\psi} & s_{\phi}c_{\theta} \\
c_{\phi}s_{\theta}c_{\psi} + s_{\phi}s_{\psi} & c_{\phi}s_{\theta}s_{\psi} - s_{\phi}c_{\psi} & c_{\phi}c_{\theta}
\end{bmatrix}. (49)$$

• Destination seeking (attractive component).

The destination seeking component of the velocity commands is defined as:

$$\begin{bmatrix} u_{\text{attr}} \\ v_{\text{attr}} \\ w_{\text{attr}} \end{bmatrix} = \begin{cases} \frac{s_{\text{d}} p_{\text{g}}}{\|p_{\text{g}}\|}, & \text{if } \|p_{\text{g}}\| \ge d_{\text{s}}, \\ \frac{s_{\text{d}} p_{\text{g}}}{d_{\text{s}}}, & \text{if } \|p_{\text{g}}\| < d_{\text{s}}, \end{cases}$$
(50)

where  $p_{\rm g}$  is the position of the destination relative to the center of mass, which is resolved in the inertial frame,  $s_d$  is the desired speed, and  $d_s$  is the stopping distance.

*Remark 4:* As can be seen from (50), the goal speed is proportional to its distance to the destination if the quadrotor

is closer than  $d_s$  to the destination. On the other hand, the goal speed is constant if the quadrotor is farther than  $d_s$  from the destination.

## C. Desired commands

The velocity commands  $u_c, v_c$ , and  $w_c$  from (45) are passed through low pass filters, which output the desired translational velocities  $u_d, v_d$ , and  $w_d$  and their derivatives. The details of the filters are described in [14]. In addition, for the nominal closed-loop system, the desired pitch and roll are determined from

$$\theta_{d} = \tan^{-1} \left[ \frac{(\dot{u}_{d} - K_{u}e_{u}) c_{\psi} + (\dot{v}_{d} - K_{v}e_{v}) s_{\psi}}{\dot{w}_{d} - K_{w}e_{w} - g} \right],$$

$$\phi_{d} = \tan^{-1} \left[ \frac{(\dot{u}_{d} - K_{u}e_{u}) c_{\theta}s_{\psi} - (\dot{v}_{d} - K_{v}e_{v}) c_{\theta}c_{\psi}}{\dot{w}_{d} - K_{w}e_{w} - g} \right],$$
(51)

where  $e_u := u - u_d$  and  $e_v := v - v_d$ . Also, u, and v, are the velocities in the x and y directions, respectively, and  $K_u$  and  $K_v$  are velocity gains. Note that the desired yaw angle  $\psi_d$  is typically set to zero and is only nonzero if the quadrotor requires rotation for pointing the object detection sensor. In this study, we assume that obstacles can be detected without the need to rotate the vehicle, therefore,  $\psi_d = 0$ .

The desired angular velocity is calculated from

$$\omega_d = Q(\dot{\Phi}_d - K_{\Phi}e_{\Phi}),\tag{52}$$

where  $e_{\Phi} := \Phi - \Phi_d$  and  $\Phi_d = [\phi_d, \theta_d, \psi_d]^{\mathrm{T}}$ . Subtracting (6) and (52) leads to

$$e_{\omega} = Q(\dot{\Phi} - \dot{\Phi}_d + K_{\Phi}e_{\Phi}) = Q(\dot{e}_{\Phi} + K_{\Phi}e_{\Phi}). \tag{53}$$

Since the controller (9) is designed such that  $\lim_{t\to\infty} e_{\omega} = 0$ , we can conclude that  $e_{\Phi}$  converges to zero.

## IV. SIMULATION RESULTS

In this section, the following three cases are simulated to illustrate the performance of our method:

- Case 1: Without saturation
- Case 2: With saturation Without AWC
- Case 3: With saturation With AWC

For the simulation, we consider the following parameters:

$$m = 1.01 \text{ kg}, l = 0.1185 \text{ m}, k = 7.5 \times 10^{-6} \text{ kg} \cdot \text{m/rad}^2,$$
  
 $b = 1.4 \times 10^{-7} \text{ kg} \cdot \text{m}^2/\text{rad}^2, \overline{\varpi} = 628 \text{ rad/s},$ 

$$I = diag(0.00585, 0.0054, 0.007), K_u = 1, K_v = 1, K_{\Phi} = I_3.$$

where l is the thrust moment arm, k is the propeller thrust constant, b is the propeller drag constant [14], and  $\overline{\varpi}$  is the maximum propeller speed. Let the guidance parameters be

$$\begin{aligned} a_{\rm i} &= 0.84 \text{ m}, \ b_{\rm i} = 0.7 \text{ m}, \ c_{\rm i} = 0.36 \text{ m}, \\ a_{\rm o} &= 1.65 \text{ m}, \ b_{\rm o} = 1.12 \text{ m}, \ c_{\rm o} = 0.83 \text{ m}, \\ s_{\rm d} &= 2.87 \text{ m/s}, \ d_{\rm s} = 2.87 \text{ m}, \ U_{\rm max} \ = 5.5 \text{ m/s}. \end{aligned}$$

The starting and the destination coordinates are [0,1.5,3] and [4,0,1.1]. The desired yaw  $\psi_d$  is set to zero. Also, to induce saturation of the propellers, a simplified wind disturbance is considered: a rectangular signal with a magnitude equivalent to 67.62% of the maximum thrust generated by a single propeller (i.e.,  $0.6762k\overline{\varpi}^2$ ) is applied in the positive y-direction over the time interval of 1s to 3s.

Remark 5: For quadrotors, the mechanism that causes saturation is propeller speed, which occurs when the motors driving the propellers reach their maximum rotational speed

and cannot increase their speed any further to generate additional thrust or torque. However, as seen from Fig. 1 the controller produces torque and thrust commands while the UAV (and AWC) are driven by the saturation (and deadzone) of the torques and thrust. Therefore, we obtain  $\operatorname{sat}_{\mathcal{I}_i}^T(T)$  and  $\operatorname{sat}_{\mathcal{I}_i}^T(\tau_i)$  by perform the following real-time operations in simulation:

$$\begin{bmatrix} \varpi_1^2 \\ \varpi_2^2 \\ \varpi_3^2 \\ \varpi_4^2 \end{bmatrix} = \begin{bmatrix} \frac{1}{4k} & \frac{1}{4kl} & \frac{1}{4k} & \frac{1}{4b} \\ \frac{1}{4k} & \frac{1}{4kl} & \frac{1}{4k} & \frac{1}{4b} \\ \frac{1}{4k} & \frac{1}{4kl} & \frac{1}{4kl} & \frac{1}{4b} \\ \frac{1}{4k} & \frac{1}{4kl} & \frac{1}{4kl} & \frac{1}{4b} \end{bmatrix} \begin{bmatrix} T \\ \tau_1 \\ \tau_2 \\ \tau_3 \end{bmatrix}.$$
 (54)

With propeller speed limited by  $\varpi_{i \text{sat}}^2 = \min\left(\max\left(\varpi_i^2,0\right),\overline{\varpi}^2\right)$ ,  $\operatorname{sat}_{\underline{T}}^{\overline{T}}(T)$  and  $\operatorname{sat}_{\underline{\tau}_i}^{\overline{\tau}_i}(\tau_i)$  are then calculated as follows:

$$\begin{bmatrix} \operatorname{sat}_{\underline{T}}^{\underline{T}}(T) \\ \operatorname{sat}_{\underline{\tau_{1}}}^{\overline{\tau_{1}}}(\tau_{1}) \\ \operatorname{sat}_{\underline{\tau_{3}}}^{\overline{\tau_{2}}}(\tau_{2}) \\ \operatorname{sat}_{\underline{\tau_{3}}}^{\overline{\tau_{3}}}(\tau_{3}) \end{bmatrix} = \begin{bmatrix} k & k & k & k \\ kl & -kl & -kl & kl \\ kl & kl & -kl & -kl \\ b & -b & b & -b \end{bmatrix} \begin{bmatrix} \varpi_{1\text{sat}}^{2} \\ \varpi_{2\text{sat}}^{2} \\ \varpi_{3\text{sat}}^{2} \\ \varpi_{4\text{sat}}^{2} \end{bmatrix},$$

$$(55)$$

from which the deadzones of the input thrust and torques can be obtained.

The LMI problems are solved using the YALMIP toolbox [17] with the MOSEK solver [18]. For simulation results, it is assumed that the conditions of Remarks 1 and 2 do not occur. Therefore, only LMIs (21) and (40) are solved to calculate the controller and AWC gains:

$$\begin{split} K_{\omega\,1} &= K_{\omega\,2} = K_{\omega\,3} = 0.9605, K_{\rm w} = 0.9019, \\ K_{a\,1} &= K_{a\,2} = K_{a\,3} = 1, K_{\bar{a}} = 1. \end{split}$$

The quadrotor trajectories and propeller speeds are illustrated in Figs 2-5. In Case 1, the green trajectory in Fig. 2 shows that the quadrotor avoids all obstacles and efficiently reaches the destination using a short route, as expected. However, it is evident from Fig. 3 that the propeller speeds exceed the maximum speed of  $\overline{\varpi}=628~\mathrm{rad/s}$ .

In Case 2, the saturation constraint is applied in simulation but AWC is not implemented. As can be seen from the blue trajectory in Fig. 2, due to the saturation of the propeller speeds (see Fig. 4), the quadrotor travels a considerably longer distance to reach its destination.

In Case 3, the saturation constraint is applied in simulation and AWC is implemented. From the red trajectory in Fig. 2, we can see that although saturation of propeller speeds occurs (see Fig. 5), the route taken by the quadrotor to reach its destination is notably shorter than that of Case 2. However, it takes a longer route compared to Case 1, which of course is the ideal case since saturation is absent. For a quantitative comparison, the distance traveled by the quadrotor in the three cases is presented in Table I.

For Case 3, the translational velocities and Euler angles are respectively plotted in Figs. 6 and 7, illustrating that these signals track the corresponding desired signals. The difference observed in tracking the desired signals of translational velocities is due to the saturation of propellers and the disturbance applied to the system.

### V. CONCLUSION

In this paper, the constrained control problem is addressed in a guidance and control scheme for quadrotors through

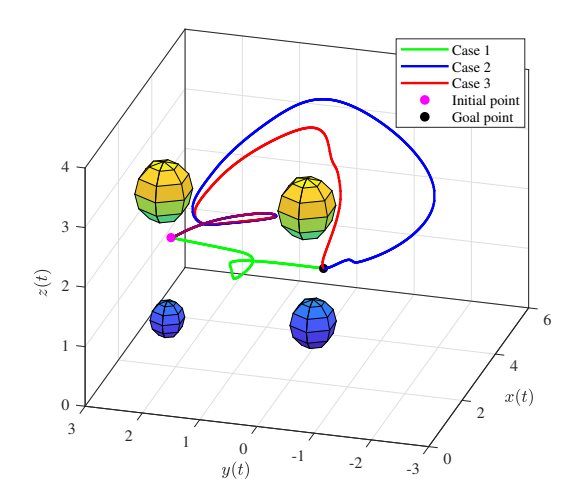


Fig. 2. Comparison of the quadrotor trajectories

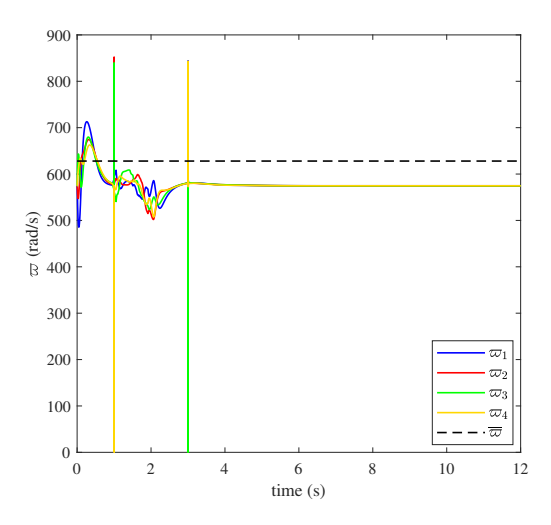
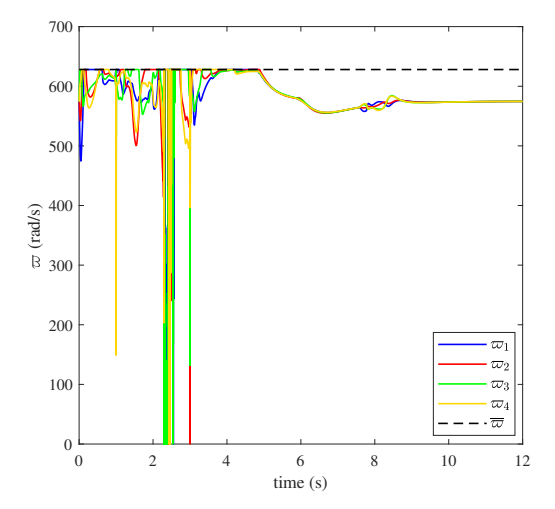


Fig. 3. Propeller speed  $\varpi$  (Case 1)



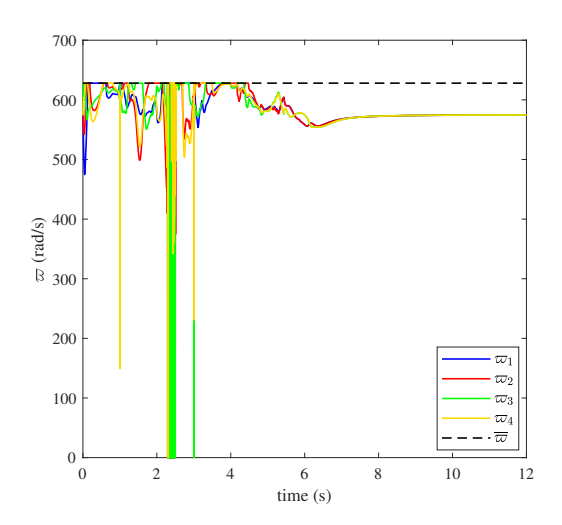


Fig. 5. Propeller speed  $\varpi$  (Case 3)

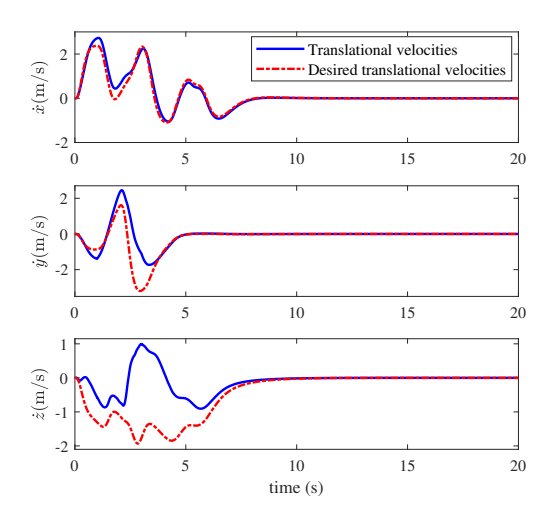


Fig. 6. Translational velocities (Case 3)

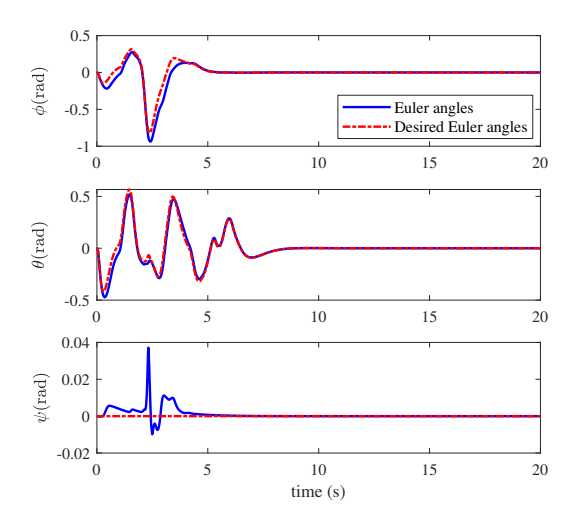


Fig. 7. Euler angles (Case 3)

TABLE I
DISTANCE TRAVELED BY QUADROTOR

Case 1	Case 2	Case 3
6.4576 (m)	15.0744 (m)	11.1839 (m)

the development of an anti-windup-based control system. Because of the coupled nonlinear dynamics which govern quadrotors, the challenge of designing an anti-windup compensator is overcome through a novel reformulation of the saturation constraints, which allows for the formulation of an LMI design solution. The effectiveness of the design method is illustrated through simulation of obstacle avoidance and destination seeking of a quadrotor in an unknown environment.

## REFERENCES

- [1] H. Jeon, J. Song, H. Lee, and Y. Eun, "Modeling quadrotor dynamics in a wind field," IEEE/ASME Transactions on Mechatronics, vol. 26, no. 3, pp. 1401–1411, 2020.
- [2] L. Yang, B. Li, W. Li, H. Brand, B. Jiang, and J. Xiao, "Concrete defects inspection and 3D mapping using CityFlyer quadrotor robot," IEEE/CAA Journal of Automatica Sinica, vol. 7, no. 4, 2020.
- [3] X. Lu and Z. Xing, "Application of iot quadrotor dynamics simulation," Electronics, vol. 11, no. 4, p. 590, 2022.
- [4] Z. Chang, H. Chu, and Y. Shao, "Quadrotor trajectory-tracking control with actuator saturation," Electronics, vol. 12, no. 3, p. 484, 2023.
- [5] O. Falkenberg, J. Witt, U. Pilz, U. Weltin, and H. Werner, "Model identification and attitude control for quadrotor mav's," in <u>International Conference on Intelligent Robotics and Applications</u>. Springer, 2012, pp. 460–471.
- [6] N. A. Ofodile and M. C. Turner, "Decentralized approaches to antiwindup design with application to quadrotor unmanned aerial vehicles," <u>IEEE Transactions on Control Systems Technology</u>, vol. 24, no. 6, pp. 1980–1992, 2016.
- [7] N. Buratti, D. Invernizzi, and M. Lovera, "Experimental validation of LMI-based anti-windup compensators for attitude control in multirotor UAVs," <u>IFAC-PapersOnLine</u>, vol. 52, no. 12, pp. 164–169, 2019.
- [8] P. Ghignoni, N. Buratti, D. Invernizzi, and M. Lovera, "Anti-windup design for directionality compensation with application to quadrotor UAVs," <u>IEEE Control Systems Letters</u>, vol. 5, no. 1, pp. 331–336, 2020.
- [9] M. C. Turner, G. Herrmann, and I. Postlethwaite, "Incorporating robustness requirements into antiwindup design," IEEE Transactions on Automatic Control, vol. 52, no. 10, pp. 1842–1855, 2007.
   [10] S. Galeani, S. Tarbouriech, M. Turner, and L. Zaccarian, "A tutorial
- [10] S. Galeani, S. Tarbouriech, M. Turner, and L. Zaccarian, "A tutorial on modern anti-windup design," <u>European Journal of Control</u>, vol. 15, no. 3-4, pp. 418–440, 2009.
- [11] S. Tarbouriech and M. Turner, "Anti-windup design: an overview of some recent advances and open problems," <u>IET control theory & applications</u>, vol. 3, no. 1, pp. 1–19, 2009.
- [12] L. Zaccarian and A. R. Teel, Modern anti-windup synthesis: control augmentation for actuator saturation. Princeton University Press, 2011, vol. 36.
- [13] S. Tarbouriech, G. Garcia, J. M. G. da Silva Jr, and I. Queinnec, Stability and stabilization of linear systems with saturating actuators. Springer Science & Business Media, 2011.
- [14] T. Kirven and J. B. Hoagg, "Autonomous quadrotor collision avoidance and destination seeking in a GPS-denied environment," <u>Autonomous</u> Robots, vol. 45, pp. 99–118, 2021.
- [15] C. M. Richards and M. C. Turner, "Combined static and dynamic anti-windup compensation for quadcopters experiencing large disturbances," Journal of Guidance, Control, and Dynamics, vol. 43, no. 4, pp. 673–684, 2020.
- [16] B. E. Farber and C. M. Richards, "Adaptive control and parameter-dependent anti-windup compensation for inertia-varying quadcopters," International Journal of Control, vol. 97, no. 2, pp. 235–248, 2024.
- [17] J. Lofberg, "YALMIP: A toolbox for modeling and optimization in MATLAB," in 2004 IEEE international conference on robotics and automation (IEEE Cat. No. 04CH37508). IEEE, 2004, pp. 284–289.
- [18] M. ApS, The MOSEK optimization toolbox for MATLAB manual. Version 10.0.44, 2023.